

Entanglement detection and quantum metrology by Stokes photon diffraction imaging

Hongyi Yu and Wang Yao*

*Department of Physics and Center of Theoretical and Computational Physics,
The University of Hong Kong, Hong Kong, China*

(Dated: May 16, 2022)

We show that far field diffraction image of spontaneously scattered Stokes photons can be used for detection of spin entanglement and for metrology of fields gradients in cold atomic ensembles. For many-body states with small or maximum uncertainty in spin-excitation number, entanglement is simply witnessed by the presence of a sharp diffraction peak or dip. Gradient vector of external fields is measured by the displacement of a diffraction peak due to inhomogeneous spin precessions, which suggests a new possibility for precision measurement beyond the standard quantum limit without entanglement. Monitoring temporal decay of the diffraction peak can also realize non-demolition probe of temperature and collisional interactions in trapped cold atomic gases. The approach can be readily generalized to cold molecules, trapped ions, and solid state spin ensembles.

PACS numbers: 03.67.Mn, 06.20.-f, 42.25.Fx, 67.85.-d

Cold atomic ensembles offer an ideal platform for the study of quantum many-body physics and for the implementation of quantum information processing [1]. With entanglement speculated as a key phenomenon in these occasions, efficient approach to detect entanglement is crucial for understanding its profound roles [2]. Spin of cold atoms is also widely used for precision measurement of external fields. A topic of current interest is quantum metrology which utilizes quantum properties and particularly entanglement in the probe system to reach measurement sensitivity beyond the standard quantum limit (SQL) [3].

To address these outstanding demands in the exploration of quantum physics and quantum technology using cold atomic ensembles, the key is efficient access to the right piece of information in the spin subspace. An ideal interface between spin and photon is offered by the process of spontaneous Stokes scattering [4–12]: with a laser driving an ensemble of atoms in Λ -configuration, a collective spin-excitation can be spontaneously converted into a Stokes photon with phase and wavevector preserved. One may thus anticipate that photon diffraction pattern can provide information on collective spin properties. Earlier studies on the diffraction of collectively emitted photons have focused on the super-radiance phenomenon (i.e. induced directional coherent radiation) in very dense atomic ensembles [13–15], or in ensembles prepared with a single excitation [16–20].

In this letter, we show that the far field diffraction image of spontaneously emitted Stokes photons can be used for detection of spin entanglement and for precision measurement of gradient vector of external fields in cold atomic ensembles. We find the strength of a sharp diffraction peak or dip measures spin pair-correlation sum and detects entanglement through pair-correlation sum rules we derive from optimal spin squeezing inequalities [28–31]. For many-body states with small or maximum uncertainty in spin-excitation number, entanglement is simply

witnessed by the presence of the peak or dip. Inhomogeneous spin precessions in a field gradient lead to displacement of the diffraction peak (dip), which can serve as a principle for vector metrology of fields gradients and for calibration of inhomogeneity in optical lattices. The gradiometer sensitivity can reach $1/N$ by using a spin-coherent-state of N unentangled atoms as the probe, which suggests a new possibility for going beyond the SQL of $1/\sqrt{N}$ without entanglement [32–35]. Motional dynamics leads to temporal decay of the diffraction peak which can be used for non-demolition probe of temperature and collisional interactions in trapped atomic gases.

Two remarkable features make this approach particularly suitable for ensembles with large number of atoms. First, regardless of the ensemble size, spin dephasing noise as a major error source only results in decay of the peak (dip) strength in a timescale equal to the dephasing time of a single spin. Second, the number of useful photons from a single copy of many-body state can be as large as its spin-excitation number for cold atomic ensembles which are typically dilute (i.e. interatomic distance comparable to or larger than optical wavelength). This approach complements existing optical methods for probing many-body quantum states [21–27], and is readily applicable in other systems including molecular ensembles, trapped ions and solid state spin ensembles.

Consider an optically thin cold atomic ensemble with a Λ level configuration where two atomic ground states $|g\rangle$ and $|s\rangle$ can be optically coupled to a common excited state $|e\rangle$ (Fig. 1 inset). The ensemble is driven by a laser with Rabi frequency Ω_L , detuning Δ and wavevector $\mathbf{k}_0 = k_0\hat{\mathbf{z}}$. We assume atomic motion can be taken as frozen in the duration of photon emission. With the laser coupling the $|s\rangle$ to $|e\rangle$ transition, an atom can go from state $|s\rangle$ to $|g\rangle$ by emitting a Stokes photon into the vacuum. When Δ is much larger than Ω_L and the excited state homogeneous line width Γ_0 , $|e\rangle$ can be adiabatically eliminated, leading

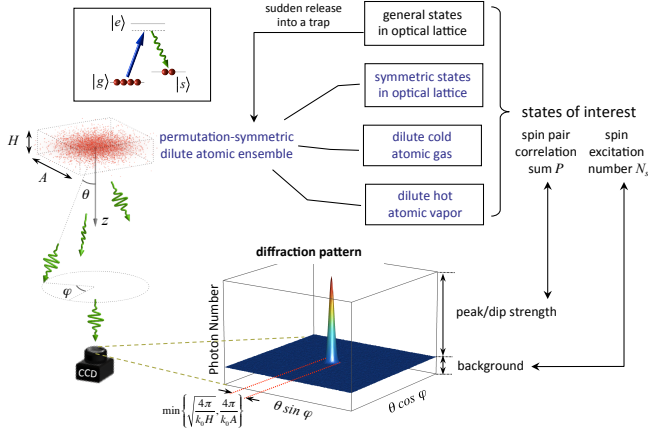


FIG. 1: Far field diffraction image of Stokes photons from permutation-symmetric dilute ensembles. The pair-correlation sum P in the many-atom state of interest manifests as a sharp diffraction peak (for $P > 0$) or dip (for $P < 0$) along the forward direction, with strength $\propto |P|$ and width inversely proportional to the ensemble size.

to the effective light-atom coupling in the electric-dipole and rotating wave approximation: $\hat{H} = \sum_{\mathbf{k}} \hbar \omega_{\mathbf{k}} \hat{a}_{\mathbf{k}}^{\dagger} \hat{a}_{\mathbf{k}} + \sum_j E_z \hat{\sigma}_j^z + \sum_{\mathbf{k}} \mathbf{g}_{\mathbf{k}} \sum_j e^{-i(\mathbf{k}-\mathbf{k}_0) \cdot \mathbf{r}_j} \hat{\sigma}_j^- \hat{a}_{\mathbf{k}}^{\dagger} + \text{h.c.}$. Here $\mathbf{g}_{\mathbf{k}} = \frac{\Omega_L}{2\Delta} \sqrt{\frac{2\pi\omega_{\mathbf{k}}}{V}} \hat{\mathbf{e}}_{\mathbf{k}} \cdot \boldsymbol{\mu}$, $\hat{\mathbf{e}}_{\mathbf{k}}$ and $\boldsymbol{\mu}$ being respectively the unit polarization vector and the single atom dipole. $\hat{\sigma}_j^- \equiv |g\rangle_j \langle s|$ and $\hat{\sigma}_j^z \equiv |s\rangle_j \langle s| - |g\rangle_j \langle g|$. We assume anti-Stokes scattering is either forbidden by the polarization selection rule or suppressed by the much larger detuning when $E_z \gg \Delta$.

Emission of a Stokes photon into mode $\mathbf{k} = (k, \theta, \varphi)$ is accompanied by the annihilation of a spin excitation by $\hat{J}^-(\Delta\mathbf{k}) \equiv \sum_{j=1}^N e^{-i\Delta\mathbf{k} \cdot \mathbf{r}_j} \hat{\sigma}_j^-$, $\Delta\mathbf{k} = \mathbf{k} - \mathbf{k}_0$. The angular distribution of the photon emission rate is given by $I(\theta, \varphi, t) = I_s(\theta) I_c(\theta, \varphi, t)$. I_s is the single atom dipole emission pattern, a slow varying function of θ . $I_c(\theta, \varphi, t) \equiv \text{Tr}[\hat{J}^+(\Delta\mathbf{k}) \hat{J}^-(\Delta\mathbf{k}) \rho(t)]$ is the collective factor where $\rho(t)$ is the atomic density matrix. At the initial time of photon emission,

$$\begin{aligned} I_c(\theta, \varphi, 0) &= \langle \hat{N}_s \rangle + \sum_{j \neq j'} e^{-i\Delta\mathbf{k} \cdot (\mathbf{r}_j - \mathbf{r}_{j'})} \langle \hat{\sigma}_{j'}^+ \hat{\sigma}_j^- \rangle \quad (1) \\ &= \langle \hat{N}_s \rangle - \frac{P}{N-1} + P \frac{|\langle \sum_j e^{-i\Delta\mathbf{k} \cdot \mathbf{r}_j} \rangle|^2}{N^2 - N}, \end{aligned}$$

where $\hat{N}_s \equiv \sum_j (\hat{\sigma}_j^z + 1)/2$ is the spin-excitation number operator. Here and hereafter $\langle \dots \rangle$ denotes the expectation value over $\rho(0)$, the initial many-body state of interest. $P \equiv \langle \sum_{j \neq j'} \hat{\sigma}_{j'}^+ \hat{\sigma}_j^- \rangle$ is the sum of spin pair-correlations. The last equal sign in Eq. (1) holds when $\rho(0)$ is invariant under permutation of atoms, which is the typical situation for atom gases. $|\langle \sum_j e^{-i\Delta\mathbf{k} \cdot \mathbf{r}_j} \rangle|^2$ is a sharp feature which equals N^2 along the forward direction ($\theta = 0$), and drops to zero for $\theta \geq \theta_b \equiv \min\left\{\sqrt{\frac{\pi}{k_0 H}}, \frac{2\pi}{k_0 A}\right\}$ where A and H are respectively the

transverse and longitudinal size of the ensemble (Fig. 1). Thus, positive (negative) pair-correlation sum manifests as a sharp diffraction peak (dip), and its magnitude can be read out from the ratio of the peak (dip) to the background: $\frac{I(\theta=0) - I(\theta_b)}{I(\theta_b)} = \frac{P}{\langle \hat{N}_s \rangle - P/N}$. For general states in optical lattices without the permutation symmetry, P can be measured after sudden release of atoms into a spin-independent trap [1]. The density matrix averaged over many ensemble copies will become permutation-symmetric after atoms lose memory of their initial positions, while P is preserved by the atomic motions. Moreover, we find that pair-correlation sum of a dilute hot atomic vapor can be measured in the same way if Stokes photon emission is controlled to be much slower than atomic motions (see supplementary material).

With the spin-excitation number conserved in most physical processes of interest, its expectation value $\langle \hat{N}_s \rangle$ and uncertainty $\Delta N_s \equiv \sqrt{\langle \hat{N}_s^2 \rangle - \langle \hat{N}_s \rangle^2}$ are usually known *a priori*. The peak (dip) to background ratio is then sufficient to detect entanglement via available spin squeezing inequalities [28–31]. The longitudinal component of total spin is equivalent to the spin-excitation number: $\hat{J}_z = \hat{N}_s - N/2$, and the second moment of transverse components is equivalent to the pair-correlation sum: $\langle \hat{J}_x^2 \rangle + \langle \hat{J}_y^2 \rangle = P + N/2$. Many spin squeezing inequalities derived for first and second moments of total spin can thus be formulated as pair-correlation sum rules. For example, the optimal spin squeezing inequalities discovered in Ref. 30 become:

$$P \leq (N-1)\Delta N_s^2, \quad (2a)$$

$$P \geq -\Delta N_s^2, \quad (2b)$$

$$(N-1)P \geq \langle \hat{N}_s^2 \rangle - N\langle \hat{N}_s \rangle. \quad (2c)$$

Violation of any one of Eq. (2a-2c) implies entanglement.

Entanglement detection based on the above pair-correlation sum rules is described by the phase diagrams shown in Fig. 2(a-c). For eigenstates of \hat{J}^2 and \hat{J}_z , the phase space characterized by the total spin quantum number J and the magnetic quantum number M consists of a peak region and a dip region, violating Eq. (2a) and (2b) respectively (Fig. 2b). States violating Eq. (2c) form a subset of the dip region (to the left of the dashed curve in Fig. 2b). For a general many-body state, the diffraction pattern is simply the weighted average of these patterns associated with definite J and M , since $\sum_{j \neq j'} \hat{\sigma}_j^+ \hat{\sigma}_{j'}^-$ does not mix states of different J and M . *Qualitative* criteria become possible for entanglement witness in two limits. With vanishing ΔN_s seeing either a diffraction peak or dip verifies entanglement, while with maximum ΔN_s seeing a dip verifies entanglement (Fig. 2(a-b)). On the other hand, a peak (dip) strength exceeding some threshold value always implies entanglement. Taking half-spin-excitation states for example, observing a dip to background ratio $|r| \geq \frac{1}{2}$ or a

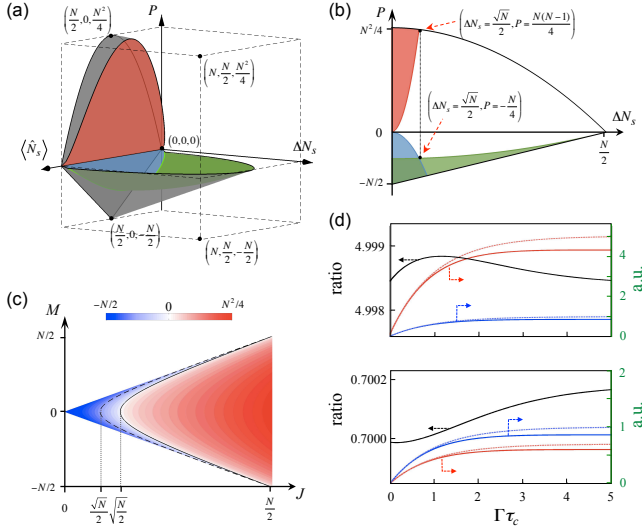


FIG. 2: (a) Phase diagram in the parameter space $(\langle \hat{N}_s \rangle, \Delta N_s, P)$. States in the surrounded region are all entangled ones. (b) A slice of (a) taken for $\langle \hat{N}_s \rangle = N/2$. The red, blue and green regions are entangled states violating inequalities Eq. (2a), (2b) and (2c) respectively. The grey surfaces in (a) and the black curves in (b) are boundaries between physical and unphysical regions. Positive and negative sections of P axis use different linear scale. (c) Strength of the diffraction peak (red) or dip (blue) for eigenstates of total spin \hat{J}^2 and \hat{J}_z . (d) Upper (lower): peak (dip) to background ratio as a function of the collection interval τ_c for a half-spin-excitation state with $P = 2.5N$ ($P = -0.35N$), shown as the black curve. The calculation is for $N = 4000$ atoms of a 2D Gaussian distribution with FWHM $A = 100 \mu\text{m}$. Peak or dip (background) strength is evaluated at $\theta = 0$ ($\theta = \frac{2\pi}{k_0 A}$), shown by the blue (red) solid curve. Dashed curves are calculations with the multiple-light scattering and dipole-dipole interaction neglected.

peak to background ratio $r \geq \frac{N(N-1)}{N+1}$ verifies entanglement for any possible ΔN_s . Moreover, P and ΔN_s can also quantify the entanglement depth in the vicinity of Dicke states [31].

Through these pair-correlation sum rules, the initial diffraction pattern detects entanglement in non-condensed atomic ensemble regardless of shape and density. Hereafter, we focus on dilute ensembles where interatomic distance is comparable to or larger than optical wavelength. Remarkably, under this condition, one can collect all Stokes photons, not only those initial ones, for measuring the pair-correlation sum in $\rho(0)$. The diffraction pattern at an arbitrary time is determined by the instantaneous atomic density matrix $\rho(t)$ which differs from $\rho(0)$. Nevertheless, in dilute ensembles, the evolution of ρ under the spontaneous emission is dominated by independent decay of spins which preserves the initial diffraction pattern (see supplementary material). Corrections from the multiple-light scattering and dipole-dipole interaction, which need nonperturbative treatment in the

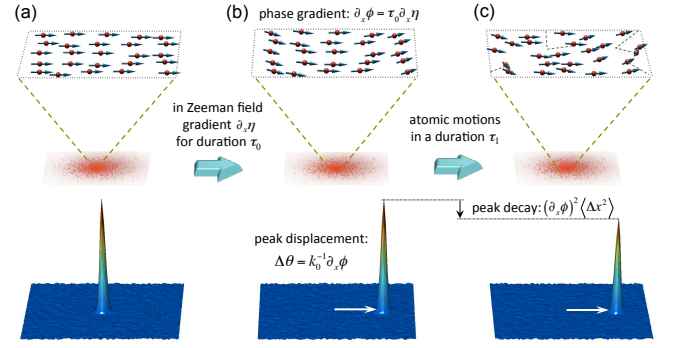


FIG. 3: Diffraction images (lower parts) from atomic ensemble in different spin configurations (upper). (a) Spin-coherent-state with in-plane polarization. (b) Evolution in a Zeeman field gradient imprints a phase gradient of spins, resulting in a displacement of the diffraction peak which can be a principle of gradiometer. (c) Atomic motions diminish the spin polarization, resulting in decay of the displaced peak. This can be a principle for non-demolition measurement of atomic temperature and collisional interactions.

dense limit [13, 14], are well accounted here by perturbation approach. We find these weak processes only result in slow varying modulation of the diffraction pattern, barely changing the ratio of the sharp peak or dip to its neighboring background. Namely,

$$r(\tau_c) \equiv \frac{n(\theta = 0, \tau_c) - n(\theta_b, \tau_c)}{n(\theta_b, \tau_c)} \cong \frac{P}{\langle \hat{N}_s \rangle - P/N} \quad (3)$$

where $n(\theta, \varphi, \tau_c) \equiv \delta\Omega \int_0^{\tau_c} dt I(\theta, \varphi, t)$ is the number of photons emitted into an infinitesimal solid angle in the collection interval $0 \leq t \leq \tau_c$. For a dilute ensemble Eq. (3) holds for arbitrarily large τ_c (cf. Fig. 2(d)).

We estimate the range of applicability of our treatment. The dilute condition is satisfied by typical cold atom gases of a density $10^{10} - 10^{12} \text{cm}^{-3}$ or by atoms in optical lattice. The duration of Stokes photon emission is of a timescale $\Gamma^{-1} = (\frac{\Omega_L}{2\Delta})^{-2} \Gamma_0^{-1}$, where Ω_L is the laser Rabi frequency and Δ the detuning. The excited state decay rate $\Gamma_0 \gtrsim 30 \mu\text{s}^{-1}$ for typical alkali atoms. [5–12] Taking $(\frac{\Omega_L}{2\Delta})^{-2} \sim 40$, all Stokes photons are emitted in a timescale $\Gamma^{-1} \lesssim \mu\text{s}$. For cold atom gases with a temperature of $1 - 100 \mu\text{K}$, the average velocity is $0.01 - 0.1 \text{m/s}$. Atoms can only travel $10 - 100 \text{nm}$ in the duration of Γ^{-1} which is indeed negligible as compared to the light wavelength.

Under free evolution, the pair-correlation changes as $\text{Tr}[\hat{\sigma}_i^+ \hat{\sigma}_i^- \rho(\tau)] = e^{i(\eta_i \tau - \gamma_i \tau)} \text{Tr}[\hat{\sigma}_i^+ \hat{\sigma}_i^- \rho(0)]$, where η_i is the Zeeman frequency and γ the homogeneous dephasing rate of an individual spin. The pair-correlation sum thus decays only at the single spin dephasing rate. Therefore entanglement in $\rho(0)$ can be reliably detected from the dephased state $\rho(\tau)$ as long as $\tau \ll \gamma^{-1}$, even when the fidelity is exponentially small with N [31].

Spatial inhomogeneity of external fields leads to posi-

tion dependent Zeeman frequency $\eta(\mathbf{r})$ and hence inhomogeneous precessions of spins. If the size of the ensemble is small compared to the variation length scale of the field, the dominating term is the gradient: $\eta(\mathbf{r}) \cong \mathbf{r} \cdot \nabla \eta$. For an ensemble initially in a permutation-symmetric state, after an interval τ_0 with frozen motion in the Zeeman field gradient, the diffraction pattern becomes $I_c = \langle \hat{N}_s \rangle - \frac{P}{N-1} + \frac{P}{N^2-N} |\langle \sum_j e^{-i(\Delta \mathbf{k} - \tau_0 \nabla \eta) \cdot \mathbf{r}_j} \rangle|^2$. We focus on situations where $\partial_z \eta$ is either zero or not picked up by atomic ensembles of a quasi-2D geometry in $x-y$ plane. The in-plane gradient simply results in a displacement of the sharp diffraction peak or dip, preserving its strength and shape (Fig. 3). This has several significant consequences. First, by evolution in an external field of known gradient, entanglement can be detected by measuring the peak or dip along a chosen direction with finite θ , such that detectors do not pick up laser photons. Second, the displacement measures the vector value of the gradient. It can thus be used as a principle of vector gradiometer of magnetic field, static electric field via dc Stark effect, and light field via ac Stark effect [11].

An ideal probe state is the spin-coherent-state of N unentangled atoms with in-plane polarization. The gradient is then probed simultaneously by the $\sim N^2$ classical pair-correlations, and its vector value is encoded as the displacement of a diffraction peak with strength $\sim N^2$. This N^2 scaling of the peak strength suggests an enhancement of the sensitivity by using large group of atoms collectively, as compared to uncorrelated probes using small groups. In a 1D geometry (Fig. 4), we find that a single collective probe using N atoms can achieve a sensitivity of $\sim \frac{1}{N} \frac{k_0}{\tau_0 \sqrt{k_0 A}}$, which goes beyond the SQL of $\sim \frac{1}{\sqrt{N}} \frac{k_0}{\tau_0 \sqrt{k_0 A}}$ for $N/2$ independent probes using atom-pairs (see supplementary material). This collectively-enhanced sensitivity with $1/N$ scaling is valid in the dilute regime $N \leq k_0 A$. Beyond this regime, the multiple light scattering can not be treated perturbatively and its effect will eventually renormalize the peak strength to the N scaling. By trapping atoms in optical lattices, the probe time τ_0 can be as long as the single spin homogeneous dephasing time, in the order of second or longer [11]. This diffraction based gradiometer using stationary atoms is immune to collective noises and uncertainty in atomic positions. In comparison, the gradiometer based on Mach-Zehnder interferometry of flying atoms in atomic fountain has the SQL sensitivity of $\sim \frac{1}{\sqrt{N}} \frac{1}{\tau_0 A}$ [36, 37], while the inevitable velocity uncertainty further sets a tighter upper bound for τ_0 dependent on the spatial resolution A (see supplementary material).

The diffraction image can also be used for non-demolition probe of atomic motions and temperature in trapped cold atom gases, by introducing a waiting time τ_1 between the imprinting of phase gradient $\nabla \phi$ on the spin-coherent-state and the measurement of the Stokes photon diffraction (Fig. 3). Atomic motions in

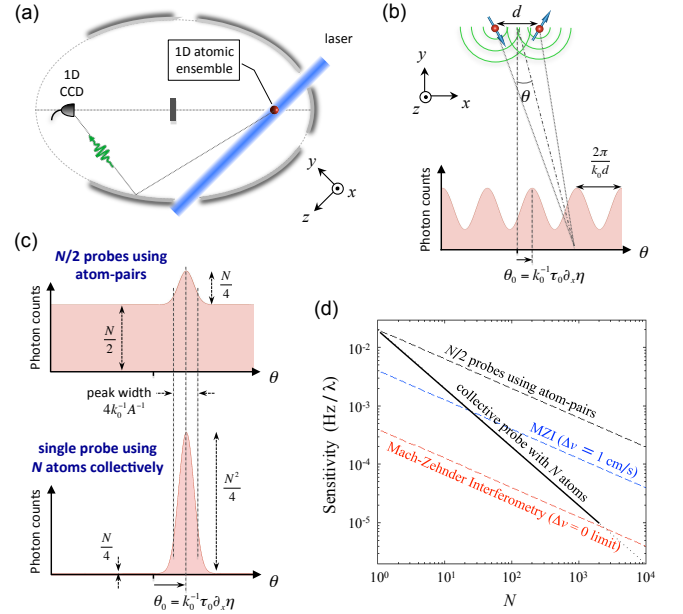


FIG. 4: Zeeman field gradiometer using a 1D atomic ensemble. (a) and (b) Schematic of the setup. The ensemble and a 1D CCD array are placed respectively on the two common focus lines of a group of elliptical cylinder mirrors. The smallest ensemble can be an atom-pair, giving a direct analog of the double-slit interferometry. (c) Signal of $\frac{N}{2}$ probes using atom-pairs (upper), and single probe using N atoms collectively (lower), with each atom placed randomly on the focus line according to a Gaussian distribution with FWHM A . The peak strength of the lower is enhanced by a factor of N . (d) Gradiometer sensitivity at a spatial resolution $A = 1$ mm with a resource of N unentangled atoms. The diffraction based gradiometer using N atoms collectively ($\frac{N}{2}$ atom-pairs independently) has a sensitivity of the $\frac{1}{N}$ ($\frac{1}{\sqrt{N}}$) scaling, shown by the solid (dashed) black line. Sensitivity of flying atom Mach-Zehnder interferometry (MZI) gradiometer is shown for reference. [36] The probe time $\tau_0 = \frac{A}{\Delta v} = 0.1$ s for the blue line, limited by a finite velocity uncertainty $\Delta v = 1$ cm/s, while $\tau_0 = 1$ s for all other lines, limited only by the single spin dephasing time.

the interval τ_1 will diminish the spin polarization, resulting in decay of the displaced diffraction peak [10]. For $|\nabla \phi|^2 \langle \Delta \mathbf{r}^2 \rangle \ll 1$, the peak strength is $\frac{N^2}{4} e^{-|\nabla \phi|^2 \langle \Delta \mathbf{r}^2 \rangle / 3}$, $\langle \Delta \mathbf{r}^2 \rangle$ being the mean square displacement of atoms. For short τ_1 when $\Delta \mathbf{r}$ is small compared to the interatomic distance d , $\langle \Delta \mathbf{r}^2 \rangle = 2 \frac{k_B T}{m} \tau_1^2$. Thus, by preparing a large phase gradient $|\nabla \phi| \sim 1/d$, the short time motion can be probed and the atomic temperature can be read out from the decay of the peak. Smaller $|\nabla \phi|$ allows the probe of long time motion which will eventually crossover to the diffusive regime by atom collisions. τ_1 is upper limited by the spin dephasing time, which is long enough for observing the entire crossover behavior from ballistic to diffusive motions, providing information about the collisional interactions in trapped gases. The collectively enhanced peak strength of $\sim N^2$ provides sufficient signal-to-noise

ratio for determining $\langle \Delta \mathbf{r}^2 \rangle$ at a given τ_1 by a single shot measurement.

WY thanks CQI at IIS of Tsinghua for hospitality during his visit through the support by NBRPC under grant 2011CBA00300 (2011CBA00301). The work was supported by the Research Grant Council of Hong Kong under grant HKU706711P and HKU8/CRF/11G.

* wangyao@hkucc.hku.hk

- [1] I. Bloch, J. Dalibard, and W. Zwerger, *Rev. Mod. Phys.* **80**, 885 (2008).
- [2] O. Guhne, and G. Toth, *Phys. Rep.* **474**, 1 (2009).
- [3] V. Giovannetti, S. Lloyd, and L. Maccone, *Science* **306**, 1330 (2004).
- [4] L.-M. Duan, M. D. Lukin, J. I. Cirac and P. Zoller, *Nature* **414**, 413 (2001).
- [5] C. H. van der Wal *et al.*, *Science* **301**, 196 (2003).
- [6] B. Julsgaard, J. Sherson, J. I. Cirac, J. F. Caronek, and E. S. Polzik, *Nature* **432**, 482 (2004).
- [7] D. N. Matsukevich *et al.*, *Phys. Rev. Lett.* **97**, 013601 (2006).
- [8] J. Simon, H. Tanji, J. K. Thompson, and V. Vuletic, *Phys. Rev. Lett.* **98**, 183601 (2007).
- [9] C.-W. Chou *et al.*, *Science* **316**, 1316 (2007).
- [10] B. Zhao *et al.*, *Nat. Phys.* **5**, 95 (2009).
- [11] U. Schnorrberger *et al.*, *Phys. Rev. Lett.* **103**, 033003 (2009).
- [12] R. Zhao *et al.*, *Nat. Phys.* **5**, 100 (2009).
- [13] Rehler and Eberly, *Phys. Rev. A* **3**, 1735 (1971).
- [14] M. Gross and S. Haroche, *Phys. Rep.* **93**, 301 (1982).
- [15] J. P. Clemens, L. Horvath, B. C. Sanders, and H. J. Carmichael, *Phys. Rev. A* **68**, 023809 (2003).
- [16] M. O. Scully, E. S. Fry, C. H. Raymond Ooi, and K. Wodkiewicz, *Phys. Rev. Lett.* **96**, 010501 (2006).
- [17] M. O. Scully and A. A. Svidzinsky, *Science* **325**, 1510 (2009).
- [18] J. H. Eberly, *J. Phys. B: At. Mol. Opt. Phys.* **39**, S599 (2006).
- [19] D. Porras and J. I. Cirac, *Phys. Rev. A* **78**, 053816 (2008).
- [20] R. Wiegner, J. von Zanthier and G. S. Agarwal, *Phys. Rev. A* **84**, 023805 (2011).
- [21] E. Altman, E. Demler, and M. D. Lukin, *Phys. Rev. A* **70**, 013603 (2004).
- [22] K. Eckert *et al.*, *Nature Physics* **4**, 50 (2008).
- [23] G. M. Bruun, B. M. Andersen, E. Demler, and A. S. Sorensen, *Phys. Rev. Lett.* **102**, 030401 (2009).
- [24] I. de Vega, J. I. Cirac and D. Porras, *Phys. Rev. A* **77**, 051804(R) (2008).
- [25] T. A. Corcovilos, S. K. Baur, J. M. Hitchcock, E. J. Mueller, and R. G. Hulet, *Phys. Rev. A* **81**, 013415 (2010).
- [26] H. Miyake *et al.*, *Phys. Rev. Lett.* **107**, 175302 (2011).
- [27] C. Weitenberg *et al.*, *Phys. Rev. Lett.* **106**, 215301 (2011).
- [28] A. S. Sorensen and K. Molmer, *Phys. Rev. Lett.* **86**, 4431 (2001).
- [29] J. K. Korbicz *et al.*, *Phys. Rev. A* **74**, 052319 (2006).
- [30] G. Toth, C. Knapp, O. Guhne and H. J. Briegel, *Phys. Rev. Lett.* **99**, 250405 (2007).
- [31] L.-M. Duan, *Phys. Rev. Lett.* **107**, 180502 (2011).
- [32] M. J. Holland and K. Burnett, *Phys. Rev. Lett.* **71**, 1355 (1993).
- [33] J. Jacobson, G. Bjork, I. Chuang, and Y. Yamamoto, *Phys. Rev. Lett.* **74**, 4835 (1995).
- [34] B. L. Higgins, D. W. Berry, S. D. Bartlett, H. M. Wiseman and G. J. Pryde, *Nature* **450**, 393 (2007).
- [35] D. Braun and J. Martin, *Nat. Commun.* **2**, 223 (2011).
- [36] M.-K. Zhou *et al.*, *Phys. Rev. A* **82**, 061602(R) (2010).
- [37] J. B. Fixler, G. T. Foster, J. M. McGuirk and M. A. Kasevich, *Science* **315**, 74 (2007).